ACS APPLIED MATERIALS & INTERFACES

Research Article

www.acsami.org

Visible-Light-Responsive TiO_2-Coated ZnO:I Nanorod Array Films with Enhanced Photoelectrochemical and Photocatalytic Performance

Yuan Wang,[†] Yan-Zhen Zheng,[†] Siqi Lu,[†] Xia Tao,*[,†] Yanke Che,[‡] and Jian-Feng Chen[§]

[†]State Key Laboratory of Organic−Inorganic Composites, Beijing University of Chemical Technology, Beijing 100029, China

[‡]Beijing National Laboratory for Molecular Sciences, Key Laboratory of Photochemistry, Institute of Chemistry, Chinese Academy of Sciences, Beijing 100190, China

[§]Research Center of the Ministry of Education for High Gravity Engineering & Technology, Beijing University of Chemical Technology, Beijing 100029, China

Supporting Information

ABSTRACT: Control of structural and compositional characteristics during fabrication of a versatile visible-light active ZnO-based photocatalyst is a crucial step toward improving photocatalytic pollutant degradation processes. In this work, we report a multifunctional photocatalytic electrode, i.e., TiO_2 coated ZnO:I nanorods (ZnO:I/TiO_2 NRs) array films, fabricated via a hydrothermal method and a subsequent wet-chemical process. This type of hybrid photocatalytic film not only enhances light absorption with the incorporation of iodine but also possesses increased electron transport capability and excellent chemical stability arising from the unique TiO_2-coated 1D structure. Owing to these synergic advantages, the degradation efficiency of the ZnO:I samples reached ∼97% after irradiation for 6 h, an efficiency 62% higher than that of pure ZnO. For RhB photocatalytic degradation experiments in both acidic (pH = 3) and alkaline (pH = 11) solutions, as well as in repeat photodegradation experiments, the ZnO:I/TiO_2 NRs films demonstrated high stability and durability under visible-light irradiation. Thus, ZnO:I/TiO_2 NRs are considered a promising photocatalytic material to degrade organic pollutants in aqueous eco-environments.

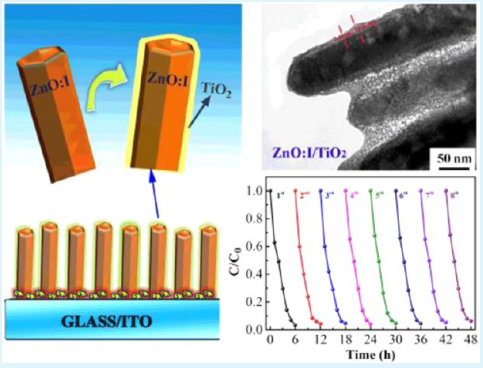

KEYWORDS: *visible light-response, TiO_2 coated ZnO:I nanorod, photoelectrochemical performance, photocatalyst*

1. INTRODUCTION

The demand of clean energy technology has attracted significant research on using nanostructured oxide semiconductors as photocatalysts for environmental purification and hydrogen generation from water splitting.[1] Among various semiconductor materials, zinc oxide (ZnO) has been regarded as one of the most promising photocatalysts owing to its wide band gap (E_g = 3.37 eV), large exciton binding energy, high carrier mobility, nontoxicity, abundant availability, simple tailoring of the nanostructures, and easy modification of the surface structure.[2] Nevertheless, there are several distinct drawbacks associated with ZnO as a photocatalyst. First, ZnO is only responsive to ultraviolet light, which occupies no more than 4% of the solar spectrum compared to visible light (43%). Second, fast recombination of photoinduced electron−hole (e^-−h^+) pairs results in low quantum efficiency and thus limits the photocatalytic potential of ZnO. Additionally, intrinsic instability of ZnO, including photocorrosion in long-term photocatalytic processes and decomposition in acidic or alkaline photoreactive media, also greatly hinders the commercialization of a ZnO photocatalyst technology.[3] The long-standing challenge remains to improve the fundamental disadvantages of ZnO as a photocatalyst for diverse applications.

Recent research has improved visible-light active ZnO materials through the incorporation of additional metal (such as Au, Ag, Zn, Cu, Al, and Pt) or nonmetal species (such as S, C, and N) to slow the recombination of photogenerated e^-−h^+ pairs,[4−12] and through fabrication of block heterojunctions with other narrow band semiconductors (such as C_3N_4, In_2S_3, CuO, and Cu_2O).[13−16] Historically, more attention has been paid to metal and nonmetal doping. In particular, iodine is thought to be the most suitable dopant for extending the light response of n-type semiconductor into the visible region. Furthermore, it has been proven that iodine anchored on the ZnO acts as electron trapping sites, thus preventing the unwanted charge recombination.[17,18] Recently, Boukherroub et al. synthesized iodine-doped ZnO (ZnO:I) nanoflower photocatalytic films for dye degradation, and they found that such hybrid films possessed significantly enhanced visible-light photocatalytic

Received: November 10, 2014
Accepted: March 5, 2015
Published: March 5, 2015

DOI: 10.1021/acsami.5b00980
ACS Appl. Mater. Interfaces 2015, 7, 6093−6101

performance in comparison to that of undoped ZnO.[19] Accordingly, a deep exploitation of a versatile ZnO:I based photocatalyst via control of structural and compositional characteristics has great significance for more effective pollutant degradation and practical application, which has yet to be reported.

In addition to the poor visible-light response, pure ZnO still suffers from insufficient electron transport and chemical instability in practical photocatalytic systems.[20] In previous works, one-dimensional (1D) ZnO nanostructures have shown improvements in electron diffusion length and charge transportation capability compared to bulk ZnO.[21−23] Meanwhile, the chemical stability of ZnO can be enhanced by coating an inert oxide layer, such as SiO_2, Al_2O_3, or TiO_2, on the surface of the ZnO.[24−26] Among them, TiO_2 is a wide-band gap semiconductor (E_g = 3.2 eV) and its energy level is similar to that of ZnO (E_g = 3.37 eV). As a result, using a TiO_2 shell onto ZnO cannot form an intrinsic surface energy barrier and hence facilitates transfer of photogenerated electrons in the composite system.[27−29] As a successful example, a composite ZnO/TiO_2 1D structure has been reported for use in an ultraviolet detection method[28] and in photovoltaic devices,[30] where a thin TiO_2 protective layer can passivate the surface trap states of the ZnO material, and at the same time, the 1D nanoarchitecture can facilitate the rapid transfer of the surface photogenerated e^-−h^+ pairs. A combination of all these features will likely produce enhanced photocatalytic and photostable activity for ZnO-based 1D materials applicable in environmental purification methods.

Given this background, we herein report a visible-light-responsive TiO_2-coated ZnO:I nanorod (ZnO:I/TiO_2 NRs) array film vertically aligned on indium tin oxide (ITO) via a hydrothermal method and a subsequent wet-chemical process. The fabricated I-doped photocatalytic 1D nanorod structure densely coated with a layer of TiO_2 was found to exhibit enhanced light absorption intensity, effective separation of photogenerated e^-−h^+, and excellent chemical stability. These photochemical and photoelectrochemical characteristics distinctly enhance the performance of the ZnO-based photocatalyst, which is further evidenced by the degradation of rhodamine B (RhB), a widely used model pollutant. More importantly, the TiO_2 coating promotes high stability and photoactivity for the ZnO:I NRs films in both acidic and alkaline solutions. Furthermore, the recycled degradation results showed that TiO_2-coated ZnO:I NRs could serve as an efficient photocatalytic material to degrade organic pollutants in aqueous eco-environments.

2. EXPERIMENTAL SECTION

2.1. Sample Preparation. All chemicals used were analytical grade reagents without any further purification steps. The ZnO:I nanorod (ZnO:I NR) array films were prepared by a two-step aqueous process. A dense ZnO seed layer was first formed by coating a solution of 0.5 M zinc acetate dehydrate ($Zn(CH_3COO)_2{\cdot}2H_2O$, Aldrich) in 2-aminoethanol and 2-methoxyethanol on an indium tin oxide (ITO) substrate, and then heated at 300 °C in air for 20 min. In the second step, vertical ZnO:I NRs gradually grew by immersing the seeded substrate in a mixed solution of 40 mM zinc nitrate hexahydrate and 40 mM hexamethylenetetramine in a neutral solution of iodic acid for a certain period of time at 92 °C. Afterward, the ZnO:I/TiO_2 NRs films were obtained by directly soaking the ZnO:I NRs films in a solution of 40 mM titanium(IV) isopropoxide dissolved in 2-propanol, followed by heat-treating at 400 °C for 30 min. The formation of the ZnO:I/TiO_2 NRs films is schematically shown in Figure 1. Pure ZnO NRs films were also obtained by the above process without the addition of iodic acid in the growth solution.

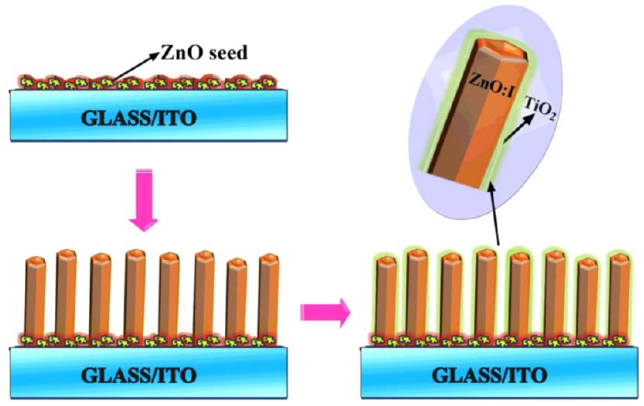

Figure 1. Schematic diagram of the formation of the ZnO:I/TiO_2 NRs array Film.

2.2. Characterization. The crystalline structure of the as-synthesized ZnO:I/TiO_2 NRs films was identified by X-ray diffraction analysis (XRD) (X'Pert PRO MPD, Panalytical) using Cu Kα radiation. The surface morphology of the ZnO:I/TiO_2 NRs films were determined from scanning electron microscope (SEM) images on a Hitachi S-4700 microscope and high-resolution transmission electron microscopy (HRTEM) images characterized on a JEOL JEM-3010 microscope. An energy-dispersive spectroscopy (EDS) measurement was performed with an X-ray energy dispersive spectrometer installed on a JEOL-6701F microscope. The absorption spectra were measured using UV−vis spectrophotometry (Lambda 950, PerkinElmer). The chemical compositions of the I-doped ZnO NRs samples were determined by X-ray photoelectron spectroscopy (XPS) performed on a thermo ESCALAB250 XPS system using an Al Kα X-ray source. The overall composition and spatial distribution of the I in an individual nanorod fragment was further investigated by scanning transmission electron microscopy elemental mapping with an X-ray energy dispersive spectrometer installed on a JEOL JEM-3010 microscope. Electrochemical and photoelectrochemical measurements were performed in a three-electrode quartz cell with a 0.1 M Na_2SO_4 electrolyte solution; a platinum wire was used as the counter electrode, a saturated calomel electrode (SCE) was used as the reference electrode, and the as-prepared photocatalyst film was used as the working electrode. The photoelectrochemical experiment results were recorded with an electrochemical system. Samples were irradiated in the visible range using a 500 W Xe lamp (Institute for Electric Light Sources, Beijing) with a 420 nm cutoff filter. Potentials are given with reference to the SCE. The on−off light photoresponse of the photocatalysts was measured at a 0.0 V bias. Electrochemical impedance spectra (EIS) were measured at 0.0 V. A sinusoidal AC perturbation of 5 mV was applied to the electrode over the frequency range of 0.05−10^5 Hz.

2.3. Photocatalytic Activity Test. The photocatalytic activity was evaluated by the decomposition of rhodamine B (RhB) dyes under visible light irradiation (λ > 420 nm) using a 500 W Xe lamp with a 420 nm cutoff filter, and the average visible light intensity was 100 mW/cm^2. The prepared films were immersed in a 40 mL aqueous solution of RhB (initial concentration, 5 × 10^{-6} mol/L). Before illumination, the RhB aqueous solution was stirred for 30 min in the dark to ensure an adsorption/desorption equilibrium was established. During degradation testing, the RhB solution with the photocatalyst film was continuously stirred using a dynamoelectric stirrer, and the concentration of RhB was monitored by colorimetry with a UV−vis spectrophotometer.

DOI: 10.1021/acsami.5b00980
ACS Appl. Mater. Interfaces 2015, 7, 6093−6101

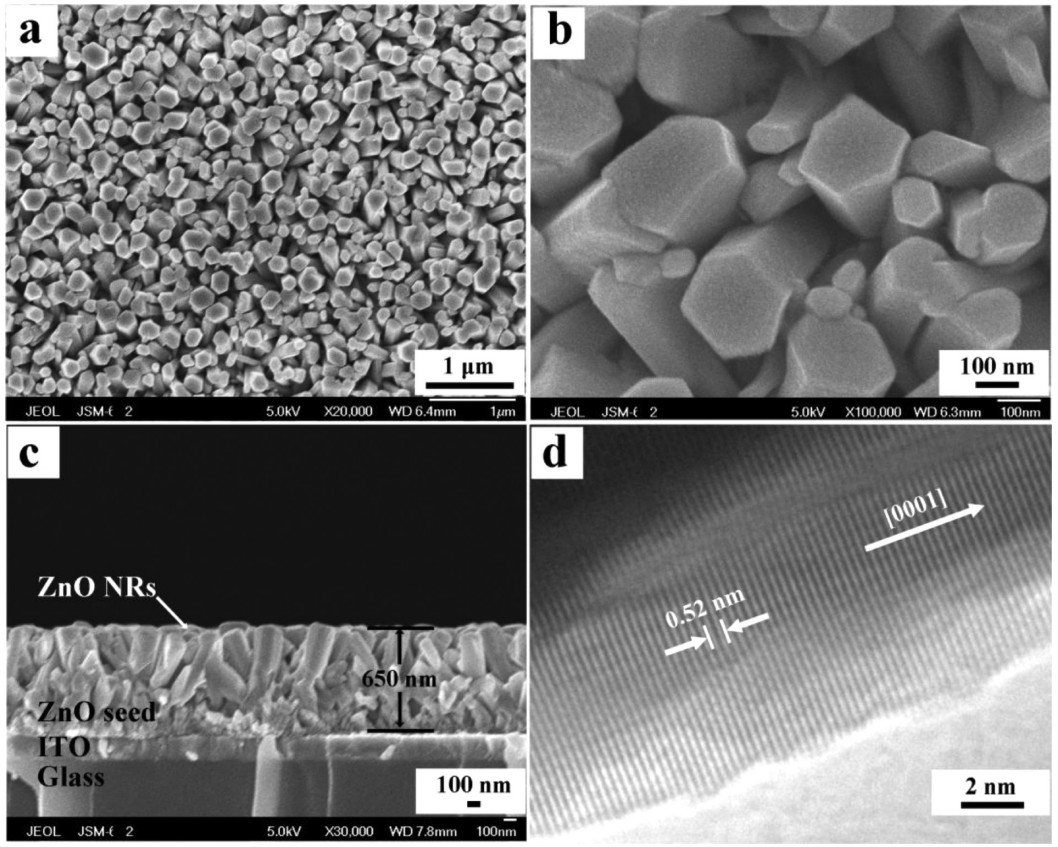

Figure 2. (a) Top view, (b) high-magnification top view, and (c) cross-sectional SEM image of as-prepared ZnO:I NRs film; (d) HRTEM image of the ZnO:I NRs.

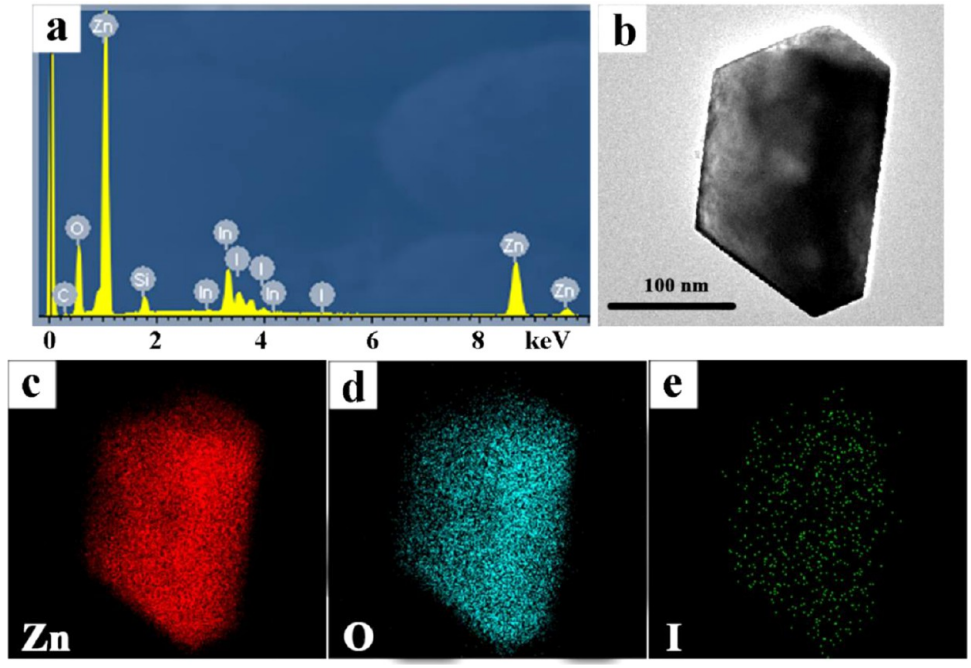

Figure 3. (a) EDS, (b) bright-field STEM image of ZnO:I NRs, and corresponding elemental mapping of (c) Zn, (d) O, and (e) I.

3. RESULTS AND DISCUSSION

3.1. Characterization of ZnO:I NRs Films. Top-view SEM images of the as-prepared ZnO:I NRs arrays, as shown in Figure 2a–b and Figure S1 (Supporting Information), show well-defined hexagonal NRs vertically grown on the ITO substrate plane. From high-magnification SEM images (Figure 1b), one can see that the diameter of ZnO:I NRs ranges from 50 to 250 nm. The length of ZnO:I NRs can be experimentally altered by adjusting the hydrothermal reaction time. By lengthening the hydrothermal growth time from 1.5 to 3.5 h,

DOI: 10.1021/acsami.5b00980
ACS Appl. Mater. Interfaces 2015, 7, 6093–6101

the rod length of ZnO:I NRs array films gradually increased, ranging from 200 to 600 nm (Figure S1a–c, Supporting Information). However, the length of the NRs remained unchanged when the hydrothermal reaction was further increased to 4.5 h (Figure S1d, Supporting Information). An optimal growth time of 3.5 h was selected for the following study. The cross-sectional SEM image in Figure 2c shows that the average thickness of the ZnO:I NRs array film is 650 nm (i.e., ZnO:I NRs plus the ZnO seed layer). The HRTEM image of a selected area of a ZnO:I NRs shows a lattice fringe of d = 0.26 nm, corresponding to the (002) plane of hexagonal wurtzite ZnO; this also implies that the ZnO:I NRs maintain the architecture of pure ZnO along the [0001] growth direction. The XRD patterns further indicated the hexagonal wurtzite structure of the ZnO:I NRs (Figure S2, Supporting Information). It is worth noting that the (002) diffraction peak of the I-doped ZnO, along with the other four peaks assigned to the (100), (101), (102), and (103) planes, clearly decreased. Such changes are likely due to the suppression of the crystal growth of the ZnO:I NRs along the c axis.[31] As a result, the length to diameter ratio of NRs decreases, which is also directly evidenced by SEM observations (Figure 2a,c and Figure S3, Supporting Information).

The presence of I and Zn in the hybrid nanostructures was confirmed by EDS analysis (Figure 3a). By scanning the ZnO:I NRs films in different areas, the average I concentration was estimated to be 0.5 mol %. The overall composition and spatial distribution of I in an individual nanorod fragment was further investigated by STEM elemental mapping. (Figure 3b–e) The elemental mappings for Zn, O, and I atoms, as shown in Figure 3c–e, indicate a homogeneous spatial distribution of the I dopant within the sample. The composition and chemical valence status of the ZnO:I NRs film was measured using XPS. Figure 4a shows a typical XPS spectrum of the ZnO:I NRs films

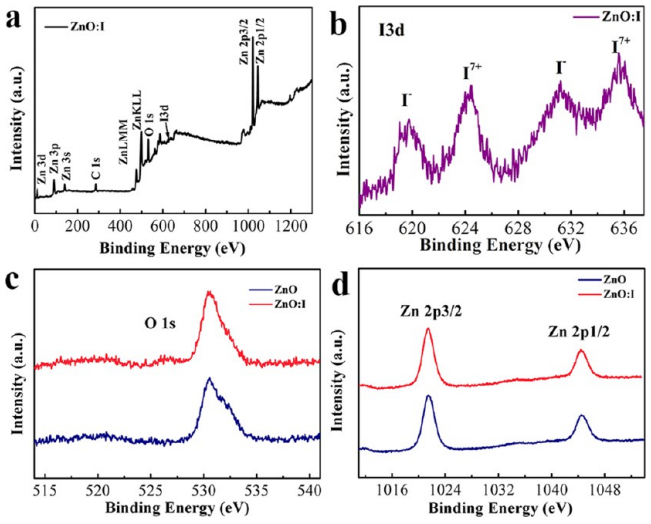

Figure 4. (a) XPS survey spectrum and (b) High resolution scan over I 3d of ZnO:I film, (c) O 1s and (d) Zn 2p for ZnO and ZnO:I film.

containing the Zn, O, and I elements. Quartet peaks of the I 3d region are observed at the approximate binding energies of 619.0, 624.0, 630.9, and 635.6 eV (Figure 4b) in accordance with recently published papers showing that 619.0 and 630.9 eV are associated with I 3d3/2 and I 3d5/2 for I^-, that 624.0 and 635.6 eV are more likely to be related to I 3d5/2 and I 3d3/2 for I^{7+}.[32−34] At approximately 623.1 eV (I^{5+}), no peak is observed, indicating that the initial species added, IO_3^- may undergo spontaneously disproportionation to the heptavalent iodine (I^{7+}) form and the negatively charged iodine (I^-) species during the hydrothermal process.[33] The binding energy peak at 529.1 eV from the O 1s spectrum of the ZnO and ZnO:I is attributed to the O^{2-} ions on the wurtzite structure of ZnO (Figure 4c). The Zn 2p peaks from ZnO and ZnO:I are observed at 1021.5 and 1044.4 eV, corresponding to the binding energy peaks of Zn 2p3/2 and Zn 2p1/2, respectively (Figure 4d). Note that no significant diffraction peak shifts of O 1s and Zn 2p for ZnO and ZnO:I were observed, indicating that the I^{7+}/I^- species do not obviously affect the inherent ZnO matrix.[35] All of the above results indicate that iodine exists in the form of I^{7+}/I^- and was successfully incorporated into the ZnO NRs framework.

3.2. Characterization of ZnO:I/TiO_2–NRs Films. The surface morphology and elemental composition of TiO_2-coated ZnO:I NRs films were investigated by SEM, EDS, and XPS. The formation of the ZnO:I/TiO_2 NRs grown on the ITO glass substrate is schematically shown in Figure 5a. The top-view SEM images of the ZnO:I/TiO_2 NRs film (Figure S4, Supporting Information) show an obvious TiO_2 coating on the ZnO:I NRs. Furthermore, high-magnification SEM images of the ZnO:I NRs (Figure 5c) and ZnO:I/TiO_2 NRs (Figure 5d) films confirm that a dense layer of TiO_2 particles is well-attached to the surface of the ZnO NRs but does not change the original structure of the ZnO:I NRs. A high-resolution TEM image (Figure 5b) further provides a clear TiO_2 outer layer surrounding ZnO:I nanorods, and the thickness of TiO_2 outer layer was determined to be 7.5–18.5 nm. Furthermore, the EDS data of the ZnO:I/TiO_2 NRs film shown in Figure 6a present Ti atomic peaks, and this also indicates that the surface of the ZnO NRs was successfully coated with TiO_2. After scanning the ZnO:I NRs films in different areas, the average Ti concentration was estimated to be 5.0 mol %. XPS was used to confirm the existence of TiO_2 on the as-grown films. Figure 6b shows the narrow range scans of the Ti 2p core level peaks of the ZnO:I/TiO_2 NRs film. The binding energies of 458.6 eV for Ti 2p3/2 and 463.2 eV for Ti 2p1/2 provide further evidence of the formation of a TiO_2 layer on the surface of the ZnO:I NRs. Moreover, the binding energy of the Ti 2p core peak of the ZnO:I/TiO_2 NRs films is assigned as a Ti–O bond (the main peak in the XPS spectra); this suggests that the chemical state of the Ti on the ZnO:I/TiO_2 NRs is Ti^{4+}.[36]

3.3. Photocatalytic Activity and Stability. The photocatalytic activity of as-prepared films was evaluated by the degradation of RhB solution under visible light irradiation ($420 < \lambda < 800$). Temporal changes in the concentrations of RhB were monitored by examining the variations in the maximal absorption peak at 554 nm in the UV–vis spectra. Figure 7a shows the temporal evolution of the spectral changes of RhB mediated by the ZnO:I/TiO_2 NRs films; the absorption peak at 554 nm decreased gradually with irradiation time and approaches zero after 6 h. Comparative experiments were also carried out to investigate the photocatalytic activity of the films with different composites under identical conditions (Figure 7b). The final degradation efficiency of the ZnO:I sample reached ~97% after 6 h of irradiation and is superior to that of the ZnO (only ~60%). Obviously, the I-doping significantly improved the photocatalytic activity of the ZnO NRs. In addition, the ZnO:I/TiO_2 NRs films not only present almost the same degradation activity but also display greatly improved photocatalytic stability in extreme environments (e.g.,

DOI: 10.1021/acsami.5b00980
ACS Appl. Mater. Interfaces 2015, 7, 6093–6101

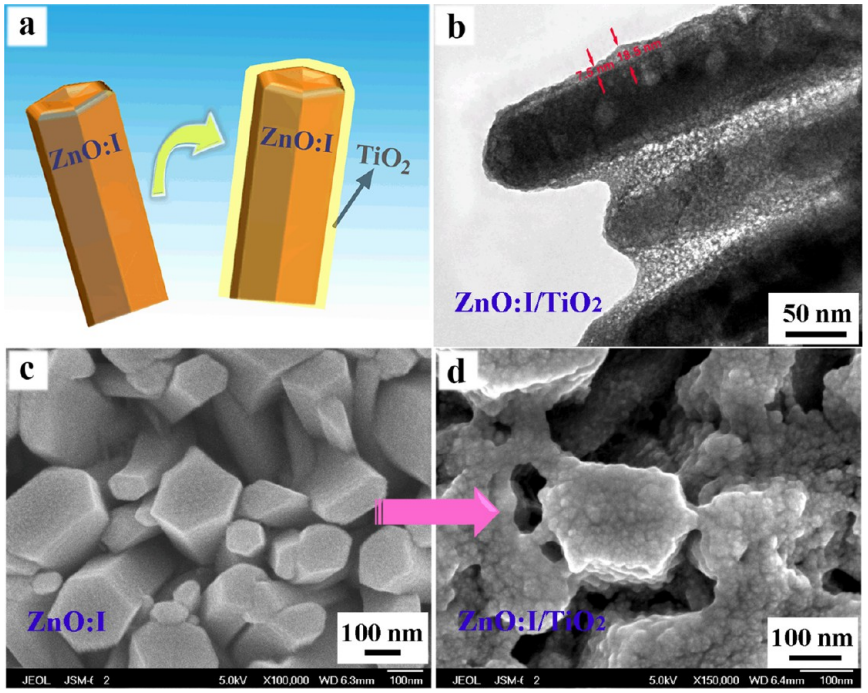

Figure 5. (a) Schematic diagram and (b) TEM image of ZnO:I/TiO_2 NRs film. High-magnification SEM images of (c) ZnO:I and (d) ZnO:I/TiO_2 NRs films.

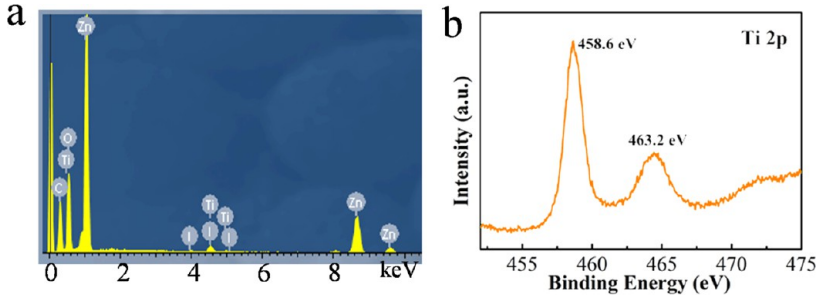

Figure 6. (a) EDS image of ZnO:I/TiO_2 NRs film and (b) high-resolution XPS spectra for Ti 2p.

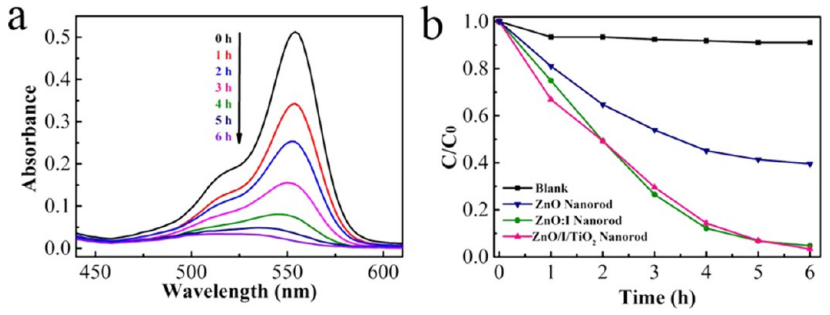

Figure 7. (a) Temporal spectrum changes of RhB taking place in the presence of ZnO:I/TiO_2 NRs film and (b) comparison of the photocatalytic degradation of RhB solution in the presence of pure ZnO, ZnO:I, ZnO:I/TiO_2 NRs, and no photocatalyst (blank) under visible light irradiation. C_0 and C are the initial concentration after adsorption equilibrium and temporal concentration of RhB at different time, respectively.

acidic or alkaline solution) in comparison with the ZnO:I NRs films without the TiO_2 coating (see below for the experimental data and detailed discussion). A blank experiment of the photodegradation of RhB in the absence of catalysts under visible light irradiation indicates that direct photolysis and adsorption effects in this system can be ignored.

In practical applications, the stability and recycling of the photocatalyst are also critical evaluation criteria. Because pH is an important operational variable in wastewater treatment, we carried out the photocatalytic degradation of RhB catalyzed by both ZnO:I NRs and ZnO:I/TiO_2 NRs films at different pHs, and the results are shown in Figure 8. The ZnO:I/TiO_2 NRs films showed excellent degradation efficiency of RhB in both acidic (pH = 3) and alkaline (pH = 11) solutions, reaching up to ~97% after 6 h of irradiation. However, the degradation efficiency for the ZnO:I NRs films was drastically less (i.e.,

DOI: 10.1021/acsami.5b00980
ACS Appl. Mater. Interfaces 2015, 7, 6093−6101

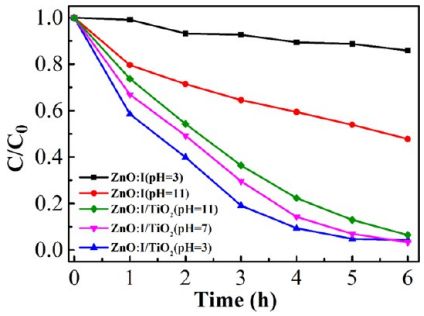

Figure 8. Photocatalytic degradation of RhB solution with different initial pHs in the presence of ZnO:I, or ZnO:I/TiO_2 NRs under visible light irradiation.

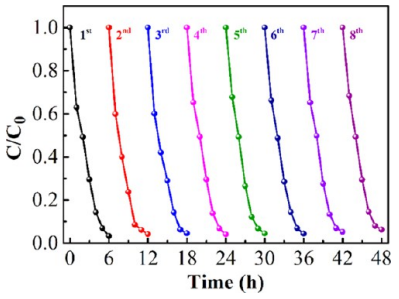

Figure 10. Cycling runs for the photodegradation of RhB in the presence of ZnO:I/TiO_2 NRs film under visible light irradiation.

~15% in the acidic solution and ~53% in the alkaline medium). The decrease in the degradation efficiency may be ascribed to chemical corrosion of the ZnO NRs in the acidic and alkaline media.[26] Clearly stated, the TiO_2 layer efficiently protects the ZnO:I NRs from damage in acidic and alkaline environments and consequently improves the stability of the photocatalyst. Further, we also observed the surface morphologies of the ZnO:I NRs and the ZnO:I/TiO_2 NRs films in both aqueous photoreaction media after a period of visible irradiation (Figure 9). From Figure 9a,b, one can clearly see that the structure of the ZnO:I NRs films was severely damaged, but the structure of the ZnO:I/TiO_2 NRs films remained mostly intact (Figure 9c,d). These results suggest that the TiO_2 layer on the surface of the ZnO:I NRs plays an important role in improving the stability of the ZnO:I NRs films during photocatalysis.

To study the lifetime of the photocatalyst, we also carried out repeated photodegradation experiments of the ZnO:I/TiO_2 NRs films in this study (Figure 10). One can see that the high photocatalytic efficiency of the ZnO:I/TiO_2 NRs films during RhB degradation was effectively maintained after the same experiment was performed eight times, indicating that ZnO:I/TiO_2 NRs films have high stability and durability under visible light irradiation.

3.4. Photoelectrochemical Performance. To reveal the light-harvesting capability of the fabricated ZnO-based films in the visible light range, we measured UV−vis absorption spectra of the pure ZnO, ZnO:I, and ZnO:I/TiO_2 NR films (Figure S5, Supporting Information). An undeniable red shift following the addition of iodine was observed. This enhanced absorption in the visible region is more likely to be induced by a sub-band gap transition corresponding to the excitation from the valence band of ZnO (E_{vb}(ZnO) = 2.89 eV, NHE) to the doped I^{7+}/I^- species ($E^0(I^{7+}/I^-)$ = 1.24 V).[31] As a result, such enhanced absorption for the ZnO:I likely explains the increase in visible light photocatalytic activity during RhB degradation as evidenced in Figure 7b. It is noted that the TiO_2-coated ZnO:I also shows enhanced absorption in the visible light

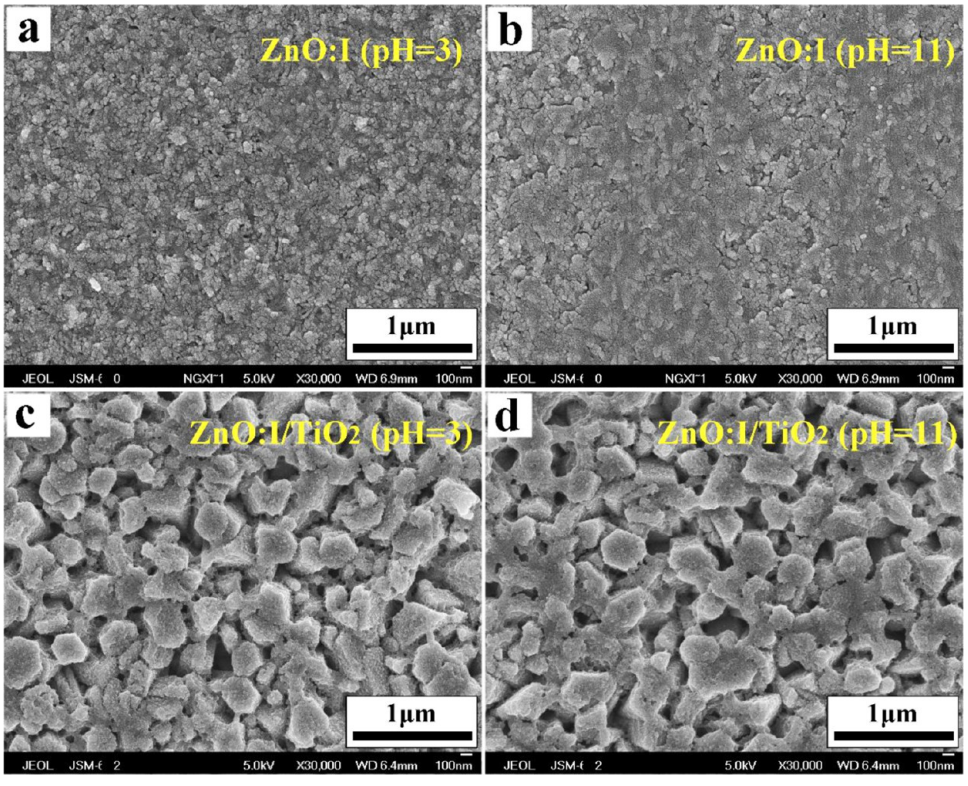

Figure 9. SEM images of ZnO:I and ZnO:I/TiO_2 films after 6 h of RhB degradation in different pHs; (a and c) pH = 3.0 and (b and d) pH = 11.0.

DOI: 10.1021/acsami.5b00980
ACS Appl. Mater. Interfaces 2015, 7, 6093−6101

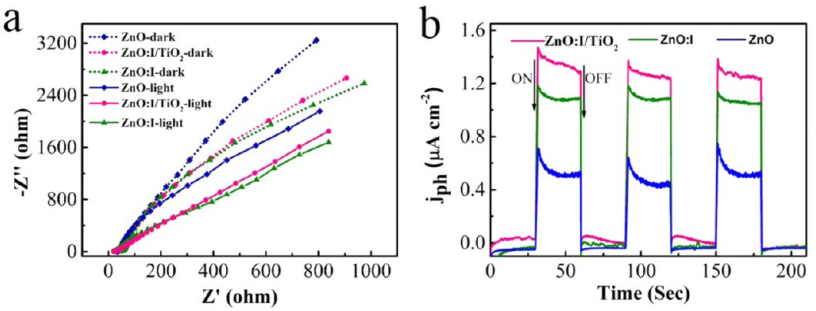

Figure 11. (a) EIS Nyquist plots of ZnO, ZnO:I, and ZnO:I/TiO_2 NRs films with light on/off cycles under the irradiation of visible light (λ > 420 nm). (b) Photoresponse of ZnO, ZnO:I, and ZnO:I/TiO_2 NRs films under visible light.

region, indicating that the TiO_2 layer does not hinder the visible absorption of the ZnO:I NRs films.

The broadened absorption is not the most important characteristic for improving the photocatalytic activity of the as-prepared films; effective separation of the photogenerated electron−hole pairs plays a more important role. The EIS Nyquist plots of as-grown samples both with and without light irradiation were carried out to investigate the interface charge separation efficiency. The radius of the arc in the EIS spectra reflects the interface layer resistance occurring at the electrode surface, and a smaller arc radius implies a higher charge transfer efficiency. As shown in Figure 11a, the impedance plots of the pure ZnO NRs, ZnO:I NRs, and ZnO:I/TiO_2 NRs electrodes cycled in a 0.1 M Na_2SO_4 electrolyte solution all exhibit semicycles within the measured frequencies. Clearly, the introduction of I leads to a significantly faster charge transfer rate indicated by a decrease in the radius of the plot compared to the pure ZnO NRs, both with and without light irradiation. The plot radius of the ZnO:I/TiO_2 NRs is slightly larger than that of the ZnO:I NRs but still much lower than the pure ZnO. The slightly lower transfer rate is likely attributed to the generation of a heterojunction between the ZnO:I NRs and the TiO_2 layer, which could hinder the electron transport process.[37]

Moreover, the transient photocurrent responses of the photocatalyst may directly correlate with the recombination efficiency of the photogenerated carriers. Figure 11b presents the results of the transient photocurrent response obtained from the pure ZnO, ZnO:I, and ZnO:I/TiO_2 NRs films. The photocurrent intensity remains constant when the light is on and rapidly decreases to zero once the light is turned off. It is clear that the photocurrent of the ZnO:I NRs is greatly improved and is approximately double that of the pure ZnO NRs. The enhanced photocurrent activity of the ZnO:I NRs films indicates more efficient separation of photoinduced electron−hole pairs and longer photogenerated charge carrier lifetimes than in the pure ZnO NRs, which could be attributed to the addition of iodine acting as trapping site for the electrons, thus inhibiting the unwanted charge recombination.[32] Furthermore, the ZnO:I/TiO_2 NRs films show enhanced photocurrent intensity, which most likely, to some extent, comes as a result of an increase in surface area with the addition of the TiO_2 layer.[38] Note that the photocurrent and absorption of the ZnO:I/TiO_2 NRs films is slight higher than that of the ZnO:I films, while the inverse result is obtained by EIS offsets its positive effect on photocatalytic activity to some degree. Thus, the ZnO:I/TiO_2 NR films show almost the same photocatalytic activity as the ZnO:I NR films for degradation of RhB. Furthermore, it is worth noting that the coating of TiO_2 outlayer enhances the stability of the ZnO:I films. As such, the excellent photocatalytic performance of the ZnO:I/TiO_2 NRs films is synergic result of enhanced light absorption with the incorporation of iodine, relatively high electron transport capability and excellent chemical stability arising from the unique TiO_2-coated 1D structure.

4. CONCLUSIONS

In summary, versatile ZnO:I/TiO_2 NRs films for use as photoelectrodes to study the photodegradation of RhB as a model pollutant were fabricated by a hydrothermal method and a subsequent wet-chemical process. The results demonstrated that the degradation efficiency of the ZnO:I/TiO_2 NRs films was significantly enhanced (~97% after 6 h of irradiation, a 62% increase over pure ZnO). The improved efficiency is attributed to the increased light absorption in the visible range and more efficient charge separation of photogenerated e^-−h^+ generated by iodine doping. The ZnO:I/TiO_2 NRs films exhibited excellent chemical stability in both acidic (pH = 3) and alkaline (pH = 11) solutions, which was further verified by repeated photodegradation experiments under visible light irradiation. This work demonstrates the possibility of fabricating high efficiency photocatalytic materials based on structural and compositional manipulation of 1D semiconducting nanomaterials.

■ ASSOCIATED CONTENT

Supporting Information

SEM images of as-prepared ZnO:I NRs films with different growth time; XRD patterns of ZnO NRs and ZnO:I NRs films; SEM images of as-prepared ZnO NRs film; and UV−vis absorption spectra of ZnO, ZnO:I, and ZnO:I/TiO_2 NR films. This material is available free of charge via the Internet at http://pubs.acs.org.

■ AUTHOR INFORMATION

Corresponding Author

* Tel: +86-10-6445-3680. Fax: +86-10-6443-4784. E-mail: taoxia@yahoo.com.

Notes

The authors declare no competing financial interest.

■ ACKNOWLEDGMENTS

The work was supported by the National Natural Science Foundation of China (Nos. 21121064, 21176019, 21377011, and 21476019), the 863 project (2013AA031901), the Specialized Research Fund for the Doctoral Program of Higher Education of China (20110010110002), and the Beijing Higher Education Young Elite Teacher Project (YETP0487).

DOI: 10.1021/acsami.5b00980
ACS Appl. Mater. Interfaces 2015, 7, 6093−6101

REFERENCES

(1) Wang, L.; Sasaki, T. Titanium Oxide Nanosheets: Graphene Analogues with Versatile Functionalities. *Chem. Rev.* **2014**, *114*, 9455−9486.

(2) Lu, X. H.; Zheng, Y. Z.; Bi, S. Q.; Wang, Y.; Tao, X.; Dai, L.; Chen, J. F. Multidimensional ZnO Architecture for Dye-Sensitized Solar Cells with High-Efficiency up to 7.35%. *Adv. Energy Mater.* **2014**, *4*, 1301802.

(3) Chen, D.; Wang, K.; Xiang, D.; Zong, R.; Yao, W.; Zhu, Y. Significantly Enhancement of Photocatalytic Performances via Core−Shell Structure of ZnO@mpg-C_3N_4. *Appl. Catal., B* **2014**, *147*, 554−561.

(4) He, W.; Kim, H. K.; Wamer, W. G.; Melka, D.; Callahan, J. H.; Yin, J. J. Photogenerated Charge Carriers and Reactive Oxygen Species in ZnO/Au Hybrid Nanostructures with Enhanced Photocatalytic and Antibacterial Activity. *J. Am. Chem. Soc.* **2014**, *136*, 750−757.

(5) Ansari, S. A.; Khan, M. M.; Ansari, M. O.; Lee, J.; Cho, M. H. Biogenic Synthesis, Photocatalytic, and Photoelectrochemical Performance of Ag-ZnO Nanocomposite. *J. Phys. Chem. C* **2013**, *117*, 27023−27030.

(6) Bera, A.; Ghosh, T.; Basak, D. Enhanced Photoluminescence and Photoconductivity of ZnO Nanowires with Sputtered Zn. *ACS Appl. Mater. Interfaces* **2010**, *2*, 2898−2903.

(7) Liang, G.; Hu, L.; Feng, W.; Li, G.; Jing, A. Enhanced Photocatalytic Performance of Ferromagnetic ZnO:Cu Hierarchical Microstructures. *Appl. Surf. Sci.* **2014**, *296*, 158−162.

(8) Ahmad, M.; Ahmed, E.; Zhang, Y.; Khalid, N. R.; Xu, J.; Ullah, M.; Hong, Z. Preparation of Highly Efficient Al-Doped ZnO Photocatalyst by Combustion Synthesis. *Curr. Appl. Phys.* **2013**, *13*, 697−704.

(9) Hidalgo-Carrillo, J.; Marinas, A.; Marinas, J. M.; Delgado, J. J.; Raya-Miranda, R.; Urbano, F. J. Water as Solvent in the Liquid-Phase Selective Hydrogenation of Crotonaldehyde to Crotyl Alcohol over Pt/ZnO: A Factorial Design Approach. *Appl. Catal., B* **2014**, *154−155*, 369−378.

(10) Bae, S. Y.; Seo, H. W.; Park, J. H. Vertically Aligned Sulfur-Doped ZnO Nanowires Synthesized via Chemical Vapor Deposition. *J. Phys. Chem. B* **2004**, *108*, 5206−5210.

(11) Wang, J.; Tsuzuki, T.; Tang, B.; Hou, X.; Sun, L.; Wang, X. Reduced Graphene Oxide/ZnO Composite: Reusable Adsorbent for Pollutant Management. *ACS Appl. Mater. Interfaces* **2012**, *4*, 3084−3090.

(12) Qin, H.; Li, W.; Xia, Y.; He, T. Photocatalytic Activity of Heterostructures Based on ZnO and N-Doped ZnO. *ACS Appl. Mater. Interfaces* **2011**, *3*, 3152−3156.

(13) Kumar, S.; Baruah, A.; Tonda, S.; Kumar, B.; Shanker, V.; Sreedhar, B. Cost-Effective and Eco-friendly Synthesis of Novel and Stable N-Doped ZnO/g-C_3N_4 Core−Shell Nanoplates with Excellent Visible-Light Responsive Photocatalysis. *Nanoscale* **2014**, *6*, 4830−4842.

(14) Khanchandani, S.; Kundu, S.; Patra, A.; Ganguli, A. K. Band Gap Tuning of ZnO/In_2S_3 Core/Shell Nanorod Arrays for Enhanced Visible-Light-Driven Photocatalysis. *J. Phys. Chem. C* **2013**, *117*, 5558−5567.

(15) Kargar, A.; Jing, Y.; Kim, S. J.; Riley, C. T.; Pan, X.; Wang, D. ZnO/CuO Heterojunction Branched Nanowires for Photoelectrochemical Hydrogen Generation. *ACS Nano* **2013**, *7*, 11112−11120.

(16) Cui, J. B.; Gibson, U. J. A Simple Two-Step Electrodeposition of Cu_2O/ZnO Nanopillar Solar Cells. *J. Phys. Chem. C* **2010**, *114*, 6408−6412.

(17) Zheng, Y. Z.; Tao, X.; Hou, Q.; Wang, D. T.; Zhou, W. L.; Chen, J. F. Iodine-Doped ZnO Nanocrystalline Aggregates for Improved Dye-Sensitized Solar Cells. *Chem. Mater.* **2011**, *23*, 3−5.

(18) Mahmood, K.; Kang, H. W.; Park, S. B.; Sung, H. J. Hydrothermally Grown Upright-Standing Nanoporous Nanosheets of Iodine-Doped ZnO (ZnO:I) Nanocrystallites for a High-Efficiency Dye-Sensitized Solar Cell. *ACS Appl. Mater. Interfaces* **2013**, *5*, 3075−3084.

(19) Barka-Bouaifel, F.; Sieber, B.; Bezzi, N.; Benner, J.; Roussel, P.; Boussekey, L.; Szunerits, S.; Boukherroub, R. Synthesis and Photocatalytic Activity of Iodine-Doped ZnO Nanoflowers. *J. Mater. Chem.* **2011**, *21*, 10982−10989.

(20) Bai, Y.; Yu, H.; Li, Z.; Amal, R.; Lu, G. Q.; Wang, L. In Situ Growth of a ZnO Nanowire Network Within a TiO_2 Nanoparticle Film for Enhanced Dye-Sensitized Solar Cell Performance. *Adv. Mater.* **2012**, *24*, 5850−5856.

(21) Che, Y. K.; Yang, X. M.; Liu, G. L.; Yu, C.; Ji, H. W.; Zuo, J. M.; Zhao, J. C.; Zang, L. Ultrathin n-Type Organic Nanoribbons with High Photoconductivity and Application in Optoelectronic Vapor Sensing of Explosives. *J. Am. Chem. Soc.* **2010**, *132*, 5743−5750.

(22) Che, Y. K.; Datar, A.; Yang, X. M.; Naddo, T.; Zhao, J. C.; Zang, L. Enhancing One-Dimensional Charge Transport through Intermolecular π-Electron Delocalization: Conductivity Improvement for Organic Nanobelts. *J. Am. Chem. Soc.* **2007**, *129*, 6354−6355.

(23) Johnson, J. C.; Knutsen, K. P.; Yan, H. Q.; Law, M.; Zhang, Y. F.; Yang, P. D.; Saykally, R. J. Ultrafast Carrier Dynamics in Single ZnO Nanowire and Nanoribbon Lasers. *Nano Lett.* **2004**, *4*, 197−204.

(24) Wang, J.; Tsuzuki, T.; Sun, L.; Wang, X. Reverse Microemulsion-mediated Synthesis of SiO_2-Coated ZnO Composite Nanoparticles: Multiple Cores with Tunable Shell Thickness. *ACS Appl. Mater. Interfaces* **2010**, *2*, 957−960.

(25) Park, J.; Shin, D. S.; Kim, D.-H. Enhancement of Light Extraction in GaN-based Light-Emitting Diodes by Al_2O_3-Coated ZnO Nanorod Arrays. *J. Alloys Comp.* **2014**, *611*, 157−160.

(26) Yeh, M. H.; Lin, L. Y.; Chou, C. Y.; Lee, C. P.; Chuang, H. M.; Vittal, R.; Ho, K. C. Preparing Core−Shell Structure of ZnO@TiO_2 Nanowires through a Simple Dipping−Rinse−Hydrolyzation Process as the Photoanode for Dye-Sensitized Solar Cells. *Nano Energy* **2013**, *2*, 609−621.

(27) Zhang, Q.; Dandeneau, C. S.; Zhou, X.; Cao, G. ZnO Nanostructures for Dye-Sensitized Solar Cells. *Adv. Mater.* **2009**, *21*, 4087−4108.

(28) Panigrahi, S.; Basak, D. Core−Shell TiO_2@ZnO Nanorods for Efficient Ultraviolet Photodetection. *Nanoscale* **2011**, *3*, 2336−2341.

(29) Pozan, G. S.; Kambur, A. Significant Enhancement of Photocatalytic Activity over Bifunctional ZnO−TiO_2 Catalysts for 4-Chlorophenol Degradation. *Chemosphere* **2014**, *105*, 152−159.

(30) Wang, M.; Huang, C.; Cao, Y.; Yu, Q.; Deng, Z.; Liu, Y.; Huang, Z.; Huang, J.; Huang, Q.; Guo, W.; Liang, J. Dye-Sensitized Solar Cells Based on Nanoparticle-Decorated ZnO/TiO_2 Core/Shell Nanorod Arrays. *J. Phys. D: Appl. Phys.* **2009**, *42*, 155104.

(31) Gomathisankar, P.; Hachisuka, K.; Katsumata, H.; Suzuki, T.; Funasaka, K.; Kaneco, S. Photocatalytic Hydrogen Production from Aqueous Na_2S + Na_2SO_3 Solution with B-Doped ZnO. *ACS Sustainable Chem. Eng.* **2013**, *1*, 982−988.

(32) Tojo, S.; Tachikawa, T.; Fujitsuka, M.; Majima, T. Iodine-Doped TiO_2 Photocatalysts: Correlation between Band Structure and Mechanism. *J. Phys. Chem. C* **2008**, *112*, 14948−14954.

(33) Su, W.; Zhang, Y.; Li, Z.; Wu, L.; Wang, X.; Li, J.; Fu, X. Multivalency Iodine Doped TiO_2: Preparation, Characterization, Theoretical Studies, and Visible-light Photocatalysis. *Langmuir* **2008**, *24*, 3422−3428.

(34) Hong, X.; Wang, Z.; Cai, W.; Lu, F.; Zhang, J.; Yang, Y.; Ma, N.; Liu, Y. Visible-Light-Activated Nanoparticle Photocatalyst of Iodine-Doped Titanium Dioxide. *Chem. Mater.* **2005**, *17*, 1548−1552.

(35) Raj, C. J.; Prabakar, K.; Karthick, S. N.; Hemalatha, K. V.; Son, M. K.; Kim, H. J. Banyan Root Structured Mg-Doped ZnO Photoanode Dye-Sensitized Solar Cells. *J. Phys. Chem. C* **2013**, *117*, 2600−2607.

(36) Peng, Y.-P.; Yassitepe, E.; Yeh, Y.-T.; Ruzybayev, I.; Shah, S. I.; Huang, C. P. Photoelectrochemical Degradation of Azo Dye Over Pulsed Laser Deposited Nitrogen-Doped TiO_2 Thin Film. *Appl. Catal., B* **2012**, *125*, 465−472.

(37) Qu, Y.; Duan, X. Progress, Challenge, and Perspective of Heterogeneous Photocatalysts. *Chem. Soc. Rev.* **2013**, *42*, 2568−2580.

(38) Manthina, V.; Correa Baena, J. P.; Liu, G.; Agrios, A. G. ZnO−TiO_2 Nanocomposite Films for High Light Harvesting Efficiency and

DOI: 10.1021/acsami.5b00980
ACS Appl. Mater. Interfaces 2015, 7, 6093−6101

Fast Electron Transport in Dye-Sensitized Solar Cells. *J. Phys. Chem. C* **2012**, *116*, 23864−23870.

DOI: 10.1021/acsami.5b00980
ACS Appl. Mater. Interfaces 2015, 7, 6093−6101